

## Investigation on grain refinement mechanism of Ni-based coating with LaAlO<sub>3</sub> by first-principles

Xuebing Zhao<sup>a</sup>, JiZhang<sup>b</sup>, Sha Liu<sup>a</sup>, Changchun Zhao<sup>a</sup>, Caixia Wang<sup>a</sup>, Xuejun Ren<sup>c</sup>, Qingxiang Yang<sup>a</sup>

<sup>a</sup>State Key Laboratory of Metastable Materials Science and Technology, Yanshan University, Qinhuangdao 066004, China <sup>b</sup> College of Mechanical Engineering, Yanshan University, Qinhuangdao 066004, China.

<sup>b</sup>School of Engineering, Liverpool John Moores University, Liverpool L3 3AF, UK

In this work, the adhesion energy, interfacial energy, interface bonding and interface magnetism of LaAlO<sub>3</sub>/Ni interface were calculated by the first-principles method. Meanwhile, the effectiveness of LaAlO<sub>3</sub> as the heterogeneous nucleus of Ni grains was also analyzed. The results show that the Wad of the AlO<sub>2</sub>-O-OT interface is the largest, which is 3.58 J/m<sup>2</sup>. Those of the LaO-OT interface and AlO<sub>2</sub>-Al-OT interface are followed. While that of the LaO-MT interface is the smallest. Interface magnetism analysis shows that the AlO<sub>2</sub>-terminated interface enhances the polarization of Ni atom, and the LaO-OT interface has a little influence on the polarization of Ni atom, while the LaO-MT interface reduces the polarization of Ni atom. The LaO-terminated interface is more stable than the AlO<sub>2</sub>-terminated interface when  $\Delta\mu_{Al}$  is low. While the AlO<sub>2</sub>-terminated interface becomes more stable when  $\Delta\mu_{Al}$  is high. When  $\Delta\mu_{Al}$  is less than -14.15 eV and -11.74 eV, the interfacial energy of the LaO-MT interface and LaO-OT interface is smaller than the liquid/solid interfacial energy of Ni ( $\sigma_{Ni(l)/Ni(s)}$ ). When  $\Delta\mu_{Al}$  is more than -9.09 eV and -6.63 eV, the interfacial energy of the AlO<sub>2</sub>-O-OT and AlO<sub>2</sub>-Al-OT interfaces is smaller than  $\sigma_{Ni(l)/Ni(s)}$ . Therefore, LaAlO<sub>3</sub> can be the heterogeneous nucleus of Ni and refine Ni grains.

### 1. Introduction

With excellent wear resistance, high-temperature oxidation and corrosion resistance, Ni-based alloy (such as NiCrBSi, Ni + WC) coatings were widely applied in mineral processing, oil exploration, cement and steel industries [1–4]. By adding hard phases into the Ni-based alloy coatings, the hardness and wear resistance of the coatings were increased simultaneously [5,6]. However, with the existence of hard phases, the toughness of the coatings was decreased. Therefore, it is significant to increase the toughness, and ensure the hardness and wear resistance of the Ni-based coatings [1,7,8].

By adding rare earth (RE) oxides (such as CeO<sub>2</sub>, La<sub>2</sub>O<sub>3</sub>), the mechanical property, corrosion resistance and oxidation resistance of the Ni-based alloy coatings are improved [9,10]. Many researches [7–13] have reported the effect of RE oxides (CeO<sub>2</sub>, La<sub>2</sub>O<sub>3</sub>) additives on the microstructure and mechanical property of the Ni-based coatings. S.P. Sharma [7] studied the influence of La<sub>2</sub>O<sub>3</sub> on the microstructure, hardness and wear behavior of flame sprayed Ni based coatings, and found that the La<sub>2</sub>O<sub>3</sub> additive can refine the grain size, and improve wear resistance of the coatings. Parisa Farahmand [8] investigated the corrosion and wear behavior of laser cladded Ni-WC coatings with the addition of La<sub>2</sub>O<sub>3</sub>. The result showed that when an optimal addition of La<sub>2</sub>O<sub>3</sub> is 1 wt.%, the grain size of Ni binder is refined and the corrosion resistance and wear resistance of the coatings can be improved. Z.Y. Zhang [11] researched the effect of CeO<sub>2</sub> on the microstructure and wear behavior of thermal spray welded NiCrWRE coatings, and indicated that the hardness and wear resistance of the coatings are significantly increased by the CeO<sub>2</sub> additive. However, the grain refinement mechanism of Ni-based coating has been rarely reported by experiment.

Currently, the first-principles calculation based on density functional theory (DFT) as an important microscopic study method has been widely used in modern science. It can not only analyze detailed atomic and electronic structures of the interface, but also calculate the interfacial adhesion work and interfacial energy, which is crucial to deeply explain the phenomena of heterogeneous nucleation [14–17]. Especially, the adhesion work and interfacial energy can reflect the binding strength and interfacial stability of the interface, which affects the heterogeneous nucleation rate directly. Han [14] calculated the interface properties of Al/TiB<sub>2</sub> interface by the first-principles method, and indicated the theoretical mechanism of TiB<sub>2</sub> as

heterogeneous nucleation of Al grains. J. Yang [15] calculated the interface adhesive energy, interfacial energy, electronic structure and bonding of austenite/LaAlO<sub>3</sub> interface, and proved that LaAlO<sub>3</sub> can be the heterogeneous nucleus of austenite and refine austenite grains. H.L. Zhang [16] investigated the structural properties of the liquid/solid interface between TiB<sub>2</sub> substrate and Al melt during heterogeneous nucleation by first-principles calculations. K. Li [17] calculated the interface properties of Mg/Al<sub>4</sub>C<sub>3</sub> interface, and analyzed the effectiveness of Al<sub>4</sub>C<sub>3</sub> as the heterogeneous nucleus of Mg grains. Therefore, in this work, the grain refinement mechanism of Ni-based coating with La<sub>2</sub>O<sub>3</sub> additive will be investigated by the first-principles method.

In the molten pool with RE oxide La<sub>2</sub>O<sub>3</sub> additive, there are many chemical reactions existing at high temperature. La<sub>2</sub>O<sub>3</sub> will transform into various La inclusions by reacting with the impurity elements Al, O and S, which indicates that La<sub>2</sub>O<sub>3</sub> can play a role for deoxidizing and desulfuring [9,18]. Our group's prophase research [19] indicated that, in various La inclusions, the formation free energy of LaAlO<sub>3</sub> is the minimum, which proves that LaAlO<sub>3</sub> is formed in the melt pool preferentially. Therefore, in the Ni-based coating with La<sub>2</sub>O<sub>3</sub> additive, whether the La inclusion LaAlO<sub>3</sub> can be the heterogeneous nucleus of Ni and refine Ni grains will be investigated in this work. In the present study, the interface adhesion energy, interfacial energy, interface bonding and interface magnetism of polar LaAlO<sub>3</sub>(100)/ Ni(100) interface were calculated by using first-principles method, which can provide theoretical basis for LaAlO<sub>3</sub> as the heterogeneous nucleus of Ni grains.

## 2. Calculation method

All calculations in this work were performed by first-principles method based on density functional theory (DFT), as implemented in the Cambridge serial total energy package (CASTEP) code. The ultrasoft pseudopotentials were employed to represent the interactions between valence electrons and ionic core. Generalized gradient approximation (GGA) of Perdew-Burke-Ernzerhof (PBE) approach was applied to describe the exchange-correlation functional [20]. Because d and f electrons exist in La atom, the strong correlation effect must be considered, in which Hubbard U was employed. The kinetic energy cut-off value [21] of 370 eV was used for plane wave expansions. The k-point sampling grids obtained by using Monkhorst-Pack method [22] were set to  $8 \times 8 \times 8$  for bulk LaAlO<sub>3</sub> and Ni,  $7 \times 7 \times 1$  for all the slabs. Surfaces and interfaces were modeled with periodic boundary conditions. Before the interface was constructed, convergence tests of LaAlO<sub>3</sub> and Ni slabs were done to determine the minimum atomic layers for meeting bulk-like interiors. A vacuum layer of 15 Å was selected for each surface and interface structure in order to eliminate the interactions between surface atoms. The Broyden-Fletcher-Goldfarb-Shannon (BFGS) [23,24] algorithm was applied to relax the models to reach the optimized structures. The energy change during the optimization finally converged to less than  $1.0 \times 10^{-5}$  eV/atom. The maximum force was 0.03 eV/Å, and the maximum displacement was  $1.0 \times 10^{-3}$  Å.

## 3. Results and discussion

### 3.1. Bulk and surface properties

#### 3.1.1. Bulk properties of LaAlO<sub>3</sub> and Ni

In order to assess the accuracy of the computation methods, a series of calculations on the bulk LaAlO<sub>3</sub> and Ni were performed firstly. The calculated optimum lattice constant of bulk LaAlO<sub>3</sub> is  $a = 3.837$  Å, which is in well agreement with the experimental value ( $a = 3.828$  Å [25]) and other reported results ( $a = 3.839$  Å [18],  $a = 3.807$  Å [26]). For bulk Ni, the calculated optimum lattice constant is  $a = 3.536$  Å, which is also in line with the experimental data ( $a = 3.52$  Å [27]) and those from literatures ( $a = 3.540$  Å [28],  $a = 3.517$  Å [29]). The spin-polarized calculations show that the magnetic moment of bulk Ni (fcc) is 0.60 μ<sub>B</sub>, which is consistent with the results reported in other literatures [29,30]. The above results indicate that the computation methods are accurate enough to guarantee the reliability of the following calculations.

### 3.1.2. Surface properties of LaAlO<sub>3</sub> and Ni

Before the interface is constructed, it is crucial to ensure that both sides of the interface are sufficiently thick to show bulk-like interiors. To determine the minimum atomic layers for meeting bulk-like interiors, convergence tests of LaAlO<sub>3</sub> (100) and Ni (100) slabs were done firstly. Ni (100) surface is non-polar surface. The surface energy of Ni (100) surface can be given by [31]:

$$\sigma = \frac{1}{2A} (E_{slab}^N - N\Delta E) \quad (1)$$

$$\Delta E = (E_{slab}^N - E_{slab}^{N-2})/2 \quad (2)$$

where N is the atomic layers of the slabs; LaAlO<sub>3</sub> (100) surface is polar surface. According to the terminated types of atoms, it can be divided into AlO<sub>2</sub>-terminated and LaO-terminated surfaces. The surface energy of LaAlO<sub>3</sub> (100) surface under Al-rich and O-rich condition can be given by:

$$\sigma = \frac{1}{2A} [E_{slab} - n_{La}\mu_{LaAlO_3}^{bulk} + (n_{La} - n_{Al})\mu_{Al}^{bulk} + (3n_{La} - n_{O})\mu_{O}^{bulk}] \quad (3)$$

Surface energy of LaAlO<sub>3</sub> (100) and Ni (100) surfaces as a function of atomic layers is listed in Table 1. From it, surface energy of Ni (100) surface converges rapidly to 2.34 J/m<sup>2</sup> for a 7 atom-layers slab, which is in well agreement with the experimental value 2.38 J/m<sup>2</sup> by Ref. [32]. For LaAlO<sub>3</sub> (100) surface, the AlO<sub>2</sub>-terminated surface and LaO-terminated surface converge to -3.44 J/m<sup>2</sup> and 7.36 J/m<sup>2</sup> when the atomic layers  $n \geq 7$ , respectively. Besides, the changes of interlayer distance in percent of bulk interlayer spacing of LaAlO<sub>3</sub> (100) surface after full relaxation were also analyzed. It is found that the atomic relaxations are mainly concentrated in the top three layers. When the atomic layers  $n \geq 7$ , the changes of the top two layers ( $\Delta 12$ ) of AlO<sub>2</sub>-terminated surface and LaO-terminated surface converge to -3.2% and +1.0%, respectively, and the slab interiors can reach bulk-like characteristics basically. The results are in linewith Ref. [18]. Therefore, according to the convergence tests, 7-layer atomstructures of LaAlO<sub>3</sub> and Ni are selected when the interface structures are built, as shown in Fig. 1. Actually, surface stability of compounds varies with different terminated types of atoms. Because of the non-stoichiometric characteristics of LaAlO<sub>3</sub> (100) surface, chemical potentials of different elements need to be considered when the surface energy is calculated. The surface energy of LaAlO<sub>3</sub> (100) surface can be given by [33,34]:

$$\sigma = \frac{1}{2A} [E_{slab} - n_{La}\mu_{La} - n_{Al}\mu_{Al} - n_{O}\mu_{O}] \quad (4)$$

where  $E_{slab}$  is the total energy of the surface structure; A is the surface area;  $n_{La}$ ,  $n_{Al}$  and  $n_{O}$  are the numbers of La, Al and O atoms in the slabs;  $\mu_{La}$ ,  $\mu_{Al}$  and  $\mu_{O}$  are the chemical potentials of corresponding atoms, respectively. After full relaxation, the surface structure will tend to an equilibrium state. Its chemical potential is equivalent to its bulk one. Therefore, the following relationships exist:

$$\mu_{\text{LaAlO}_3}^{\text{bulk}} = \mu_{\text{La}} + \mu_{\text{Al}} + 3\mu_{\text{O}} \quad (5)$$

$$\Delta H_{\text{LaAlO}_3} = \mu_{\text{LaAlO}_3}^{\text{bulk}} - \mu_{\text{La}}^{\text{bulk}} - \mu_{\text{Al}}^{\text{bulk}} - 3\mu_{\text{O}}^{\text{bulk}} \quad (6)$$

where  $\mu_{\text{LaAlO}_3}^{\text{bulk}}$  is the total energy of bulk LaAlO<sub>3</sub>;  $\mu_{\text{La}}^{\text{bulk}}$ ,  $\mu_{\text{Al}}^{\text{bulk}}$  and  $\mu_{\text{O}}^{\text{bulk}}$  are the total energy of La, Al and O atoms in the pure metal La, Al and oxygen, respectively;  $\Delta H_{\text{LaAlO}_3}$  is the heat of formation of bulk LaAlO<sub>3</sub>, which is taken to be  $-17.89$  eV/unit in this study. Combining Eq. (4) with Eq. (5),  $\mu_{\text{La}}$  can be eliminated to obtain the following equation:

$$\sigma = \frac{1}{2A} \left[ E_{\text{slab}} - n_{\text{La}}\mu_{\text{LaAlO}_3}^{\text{bulk}} + (n_{\text{La}} - n_{\text{Al}})\mu_{\text{Al}} + (3n_{\text{La}} - n_{\text{O}})\mu_{\text{O}} \right] \quad (7)$$

Because the actual condition is O-rich condition,  $\mu_{\text{O}}$  is equal to  $1/2 \mu_{\text{O}_2}^{\text{bulk}}$ . With the relationship of  $\Delta\mu_{\text{Al}} = \mu_{\text{Al}} - \mu_{\text{Al}}^{\text{bulk}}$ , Eq. (7) becomes:

$$\sigma = \frac{1}{2A} \left[ E_{\text{slab}} - n_{\text{La}}\mu_{\text{LaAlO}_3}^{\text{bulk}} + (n_{\text{La}} - n_{\text{Al}})\mu_{\text{Al}}^{\text{bulk}} + \frac{1}{2}(3n_{\text{La}} - n_{\text{O}})\mu_{\text{O}_2}^{\text{bulk}} + (n_{\text{La}} - n_{\text{Al}})\Delta\mu_{\text{Al}} \right]$$

In addition, the chemical potentials of La, Al and O atoms in the slabs must be smaller than those in their bulk phases, or the slabs would be unstable to decompose into the elemental phases immediately. Therefore, the following equation can be given:

Combined with Eqs. (5), (6), (9), the minimum and maximum values of  $\Delta\mu_{\text{Al}}$  can be given

$$\Delta\mu_i = \mu_i - \mu_i^{\text{bulk}} \leq 0 (i = \text{La, Al, O}) \quad (9)$$

Combined with Eqs. (5), (6), (9), the minimum and maximum values of  $\Delta\mu_{\text{Al}}$  can be given by:

$$\Delta H_{\text{LaAlO}_3} \leq \Delta\mu_{\text{Al}} \leq 0 \quad (10)$$

The surface energy of LaAlO<sub>3</sub> (100) surface as a function of Al chemical potential ( $\Delta\mu_{\text{Al}}$ ) is shown in Fig. 2. From it, with the increase of  $\Delta\mu_{\text{Al}}$ , the surface energy of LaO-terminated surface increases gradually, while that of AlO<sub>2</sub>-terminated one decreases. When  $\Delta\mu_{\text{Al}}$  is low, the surface energy of LaO-terminated surface is lower than that of the AlO<sub>2</sub>-terminated one, which indicates that it is more stable than the latter. However, when  $\Delta\mu_{\text{Al}}$  is high, the surface energy of AlO<sub>2</sub>-terminated surface is lower than that of LaO-terminated one, which indicates that the AlO<sub>2</sub>-terminated surface becomes more stable.

## 3.2. Interface properties between LaAlO<sub>3</sub> and Ni

### 3.2.1. Interface geometry

According to the results of convergence tests, the LaAlO<sub>3</sub>/Ni interface model was built with a  $1 \times 1$  superlattice geometry, in which a 7-layer LaAlO<sub>3</sub> (100) slab and a 7-layer Ni (100) slab are combined with the orientation relationship: LaAlO<sub>3</sub>[011]/Ni[011] and LaAlO<sub>3</sub>(100)/Ni(100). The lattice mismatch ( $\delta$ ) between LaAlO<sub>3</sub> and Ni was calculated by Bramfitt planar lattice misfit formula [35], as listed in Table 2. From it, the mismatch between LaAlO<sub>3</sub> surface and Ni surface is 8.5%, which indicates that the interface between LaAlO<sub>3</sub> and Ni is a semi-coherent interface. Therefore, the coherent interface approximation is invoked to accommodate the periodic boundary conditions, in which the softer Ni is stretched to match the dimensions of

LaAlO<sub>3</sub>. In addition to considering different types of terminations, the stacking sequences of interfacial atoms were taken into account when the interface model is built. In this work, there are two stacking sequences: OT and MT. For the AlO<sub>2</sub>-terminated interface, Al-OT indicates that the interfacial Ni atoms of Ni side are located on the top of Al atom and vacancy in the surface of LaAlO<sub>3</sub> side. O-OT represents that the Ni atoms of Ni side are placed on the top of O atoms in the surface of LaAlO<sub>3</sub> side. For the LaO-terminated interface, OT indicates that the interfacial Ni atoms of Ni side reside directly on the top of La atom and O atom in the surface of LaAlO<sub>3</sub> side. MT represents that the Ni atoms of Ni side are located on top of the middle of surface atoms of LaAlO<sub>3</sub> side. The model geometry of LaAlO<sub>3</sub>(100)/Ni(100) interface is shown in Fig. 3.

### 3.2.2. Interface adhesion

Binding strength of the interface can be judged by the work of adhesion ( $W_{ad}$ ), which is defined as the reversible work when an interface is separated into two free surfaces.  $W_{ad}$  of the interface can be given by [14,15,36–37]:

$$W_{ad} = E_{LaAlO_3} + E_{Ni} - E_{LaAlO_3/Ni} \quad (11)$$

where  $E_{LaAlO_3}$  and  $E_{Ni}$  are the total energy of LaAlO<sub>3</sub> slab and Ni slab, respectively;  $E_{LaAlO_3/Ni}$  is the total energy of the interface system;  $A$  is the interface area. Before we relaxed the LaAlO<sub>3</sub>/Ni interface model, the initial interface separation  $d_0$  was set to be 1.919 Å, which is equal to the interlayer distance of LaAlO<sub>3</sub> substrate. After full relaxation of the interface model, the interface separation  $d_0$  can be obtained from the distance of interfacial atoms of LaAlO<sub>3</sub> side and Ni side. The optimal  $W_{ad}$  and  $d_0$  values for the relaxed geometries of the four LaAlO<sub>3</sub>/Ni interfaces are listed in Table 3. From Table 3, the  $W_{ad}$  of the four LaAlO<sub>3</sub>/Ni interfaces exhibits the following sequence: AlO<sub>2</sub>-O-OT interface > LaO-OT interface > AlO<sub>2</sub>-Al-OT interface > LaO-MT interface. It is obvious that the AlO<sub>2</sub>-O-OT interface exhibits the largest  $W_{ad}$  (3.58 J/m<sup>2</sup>) and the smallest interfacial separation  $d_0$  (2.046 Å), which indicates that the binding of the AlO<sub>2</sub>-O-OT interface is the strongest in all the interfaces. The  $W_{ad}$  of the LaO-OT interface follows, which is 3.07 J/m<sup>2</sup>. While the LaO-MT interface exhibits the smallest  $W_{ad}$  (1.76 J/m<sup>2</sup>), as well as the largest  $d_0$  (2.461 Å). These may all be related with the bonding type of the interfacial atoms.

### 3.2.3. Interface stability

Generally, the lower the interfacial energy is, the more stable the interface is. The interfacial energy  $\gamma$  can be given by Ref. [38,39]:

$$\gamma = \sigma_{LaAlO_3} + \sigma_{Ni} - W_{ad} \quad (12)$$

where  $\sigma_{LaAlO_3}$  and  $\sigma_{Ni}$  are the surface energy of LaAlO<sub>3</sub> (100) and Ni (100) surfaces, respectively;  $W_{ad}$  is the work of adhesion of LaAlO<sub>3</sub>/Ni interface. The interfacial energy as a function of  $\Delta\mu_{Al}$  for the four LaAlO<sub>3</sub>/Ni interfaces is shown in Fig. 4, in which the level dotted line is the liquid/ solid interfacial energy of Ni ( $\sigma_{Ni(l)/Ni(s)}$ ). From Fig. 4, when  $\Delta\mu_{Al}$  is low, the interfacial energy of LaO-terminated interfaces is lower than that of the AlO<sub>2</sub>-terminated ones, which indicates that the LaO-terminated interface is more stable than the latter. With the increase of  $\Delta\mu_{Al}$ , the interfacial energy of AlO<sub>2</sub>-terminated interfaces decreases gradually, while that of LaO-terminated ones increases. When  $\Delta\mu_{Al}$  is high, the interface stabilities overturn, in which the interfacial energy of AlO<sub>2</sub>-terminated interfaces is lower than that of the LaO-terminated ones, which indicates that the AlO<sub>2</sub>-terminated interface becomes more stable. Besides, for the AlO<sub>2</sub>-terminated interface, in the entire range of  $\Delta\mu_{Al}$ , the interfacial energy of AlO<sub>2</sub>-O-OT interface is lower than that of the AlO<sub>2</sub>-Al-OT interface, which indicates that it is more stable than the latter. While for the LaO-terminated interface, the interfacial energy of LaO-OT interface is lower than that of the LaO-MT interface, which indicates that the LaO-OT interface is more stable. The results are in line with the above analysis results of  $W_{ad}$ .



### 3.2.4. Electronic structure and bonding

The binding of interfacial atoms depends on the electronic structure and bonding of the interface, which can be discussed by charge density, charge density difference and Mulliken population analysis in this work.

### 3.2.4. Electronic structure and bonding

The binding of interfacial atoms depends on the electronic structure and bonding of the interface, which can be discussed by charge density, charge density difference and Mulliken population analysis in this work. The charge density difference can be given by:

$$\Delta\rho = \rho_{\text{total}} - \rho_{\text{LaAlO}_3(100)} - \rho_{\text{Ni}(100)} \quad (13)$$

where  $\rho_{\text{total}}$  is the self-consistent charge density of the total LaAlO<sub>3</sub>/Ni interface system;  $\rho_{\text{LaAlO}_3(100)}$  and  $\rho_{\text{Ni}(100)}$  are the non-self-consistent charge densities of isolated LaAlO<sub>3</sub> (100) slab and Ni (100) slab, respectively. The charge density distributions and the charge density differences for the LaAlO<sub>3</sub>/Ni interfaces are shown in Figs. 5 and 6, respectively. It is obvious that chemical bonds are formed between interfacial atoms of LaAlO<sub>3</sub> side and Ni side in all the interfaces, while the bonding strength is different. From Fig. 5(a), a relatively weak chemical bond is formed in the AlO<sub>2</sub>-Al-OT interface. In Fig. 6(a), a wide range of charge depletion region exists in the interfacial Al atom. The lost charge transfers to the interface and mixes with that from the Ni atom of Ni side, which proves the formation of covalent/metallic bond. For the LaO-OT interface, in Fig. 5(b), the charge accumulation between the interfacial O atom and Ni atom indicates that the covalent bond with considerable strength is formed at the interface. While the charge accumulation between the interfacial La atom and Ni atom indicates the formation of metallic/covalent bond. From Fig. 6(b), charge depletion region exists in the interfacial Ni atom of Ni side, and charge accumulation region exists in the interfacial O atom of LaAlO<sub>3</sub> side, which proves that the ionic bond is formed between interfacial Ni atom and O atom. While the charge accumulation between the interfacial La atom and Ni atom proves the point of Fig. 5(b) once again. For the AlO<sub>2</sub>-O-OT interface, in Fig. 5(c), the obvious charge accumulation between the interfacial O atom and Ni atom indicates the formation of strong covalent bond. Its interfacial separation is relatively small. From Fig. 6(c), a wide range of charge depletion region exists in the interfacial Ni atom. The lost charge transfers to the O atom of LaAlO<sub>3</sub> side, which indicates that a polar covalent bond is formed in the interface. This partly explains the reason that the AlO<sub>2</sub>-O-OT interface exhibits the largest Wad. For the LaO-MT interface, Figs. 5(d) and 6(d) both indicate that the chemical bond formed in the interface is not obvious, which explains the reason that the LaO-MT interface exhibits the smallest Wad and the largest  $d_0$ . To further clarify the bonding characteristics of the LaAlO<sub>3</sub>/Ni interfaces, the Mulliken bond population was analyzed, as listed in Table 4.

From Table 4, for the AlO<sub>2</sub>-Al-OT interface, the overlap population of Al-Ni(Al-OT) bond is 0.29, which indicates that the covalent bond is formed between interfacial Al atom and Ni atom. While the population of O-Ni(MT) bond is 0.15, which indicates the formation of a weak covalent bond between interfacial O atom and MT-Ni atom. Combined with the above analysis results of charge density and charge density difference, the bonding of the AlO<sub>2</sub>-Al-OT interface is mainly covalent. For the LaO-OT interface, the bond overlap population of La-Ni(La-OT) bond is -1.04. From the point of view of molecular orbital theory, it can be explained as the electrostatic repulsion between charged La atom and Ni atom, which suggests the formation of metallic bond between La and Ni atoms [40]. The population of O-Ni(O-OT) bond is 0.22, which indicates the formation of covalent bond between interfacial O atom and Ni atom. Therefore, the bonding of the LaO-OT interface is a mixture of covalent bond, ionic bond and metallic bond. For the AlO<sub>2</sub>-O-OT interface, the overlap population of Al-Ni bond is 0.18, which indicates the formation of covalent bond. However, the O-Ni bond exhibits the largest population (0.46) and the smallest bond length (1.970 Å), which proves that the strong covalent bond is formed between interfacial O atom and Ni atom. Therefore, the bonding of the AlO<sub>2</sub>-O-OT interface is covalent and ionic.

### 3.2.5. Interface magnetism

The Spin-polarized partial DOS for atoms of the four LaAlO<sub>3</sub>/Ni interfaces and the bulk Ni are shown in Fig. 7(a–e). From them, the Ni PDOSs of the four interfaces are strongly different from that of the bulk one, while all Ni atoms are in ferromagnetic state in all the structures. The calculated up and down DOSs of interfacial O, Al and La atoms are almost symmetric, which indicates that these atoms are weakly polarized and their magnetic moments are negligible. The spin magnetic moments for various Ni atoms are shown in Fig. 7(f). Generally, the larger the magnetic moment is, the stronger the exchange force is, which can result in the shorter bond length and the larger bond energy [41].

For the AlO<sub>2</sub>-Al-OT interface, the spin magnetic moments of Al-OT Ni atom and MT Ni atom are 0.68  $\mu_B$  and 0.96  $\mu_B$ , respectively. They are both larger than that of the bulk Ni, which is 0.60  $\mu_B$ . While the magnetic moment of Ni atom of the AlO<sub>2</sub>-O-OT interface is 0.76  $\mu_B$ , which is also larger than that of the bulk one. These results indicate that the formation of AlO<sub>2</sub>-terminated interface enhances the polarization of Ni atom. For the LaO-OT interface, the magnetic moments of O-OT Ni atom and La-OT Ni atom are 0.68  $\mu_B$  and 0.42  $\mu_B$ , respectively. The average value is 0.55  $\mu_B$ , which differs slightly from that of the bulk Ni. However, the magnetic moment of Ni atom of the LaO-MT interface is 0.32  $\mu_B$ , which is far less than that of the bulk Ni. This indicates that the formation of LaO-MT interface reduces the polarization of Ni atom.

### 3.3. Heterogeneous nucleation analysis of Ni/LaAlO<sub>3</sub>

S.P. Sharma [7] investigated the influence of La<sub>2</sub>O<sub>3</sub> additive on the microstructure and wear behavior of NiCrBSi coatings, and proved that the La<sub>2</sub>O<sub>3</sub> additive can refine the grain size of Ni binder, as shown in Fig. 8. Bramfitt misfit theory [35] indicates that, during heterogeneous nucleation, the nucleus with  $\delta \leq 6\%$  is the most effective, and the nucleus with  $6\% < \delta \leq 12\%$  is medium effective, while the nucleus with  $\delta > 12\%$  is ineffective. According to the orientation relationship in this work, the mismatch between LaAlO<sub>3</sub> (100) surface and Ni (100) surface is 8.5%, which proves that LaAlO<sub>3</sub> as the heterogeneous nucleus of Ni is medium effective. During the solidification, to make LaAlO<sub>3</sub> as the heterogeneous nucleus of Ni, the interfacial energy of LaAlO<sub>3</sub>/Ni interface must be smaller than the liquid/solid interfacial energy of Ni, which is 0.265 J/m<sup>2</sup> [42], as shown by the level dotted line in Fig. 4. From Fig. 4, in the most range of  $\Delta\mu_{Al}$ , the interfacial energy of LaAlO<sub>3</sub>/Ni interfaces is smaller than that between primary Ni phase and Ni melt ( $\sigma_{Ni(l)/Ni(s)}$ ). Specifically, when  $\Delta\mu_{Al}$  is less than -14.15 eV and -11.74 eV, the interfacial energy of the LaO-MT interface and LaO-OT interface is smaller than 0.265 J/m<sup>2</sup>, respectively. When  $\Delta\mu_{Al}$  is more than -9.09 eV and -6.63 eV, the interfacial energy of the AlO<sub>2</sub>-O-OT and AlO<sub>2</sub>-Al-OT interfaces is smaller than 0.265 J/m<sup>2</sup>, respectively. On these conditions, LaAlO<sub>3</sub> can be the heterogeneous nucleus of Ni and refine Ni grains. Moreover, although the calculations in this work were performed at 0 K, it has been confirmed that temperature has little influence on the interface stability [43]. Therefore, the calculated results at 0 K are credible to analyze the related experimental interfaces at high temperature.

### 4. Conclusions

The interface adhesion energy, interfacial energy, interface bonding and interface magnetism of LaAlO<sub>3</sub>/Ni interface were calculated by the first-principles method in this work, which aimed at analyzing the effectiveness of LaAlO<sub>3</sub> as the heterogeneous nucleus of Ni grains. Four interface structures of AlO<sub>2</sub>-Al-OT, AlO<sub>2</sub>-O-OT, LaO-OT and LaO-MT were taken into account in this work. The conclusions are given as follows:

(1) When the atomic layers  $n \geq 7$ , both LaAlO<sub>3</sub> (100) slab and Ni (100) slab reach bulk-like characteristics basically. For LaAlO<sub>3</sub> (100) surface, when  $\Delta\mu_{Al}$  is low, the LaO-terminated surface is more stable. AlO<sub>2</sub>-terminated surface becomes more stable. (2) For the four LaAlO<sub>3</sub>/Ni interfaces, the  $\gamma$  of the AlO<sub>2</sub>-O-OT interface is the largest, which is 3.58 J/m<sup>2</sup>. Those of the LaO-OT interface and AlO<sub>2</sub>-Al-OT interface are followed, which are 3.07 J/m<sup>2</sup> and 2.24 J/m<sup>2</sup>, respectively. While that of the LaO-MT interface is the smallest, which is 1.76 J/m<sup>2</sup>. The charge density, charge density difference and Mulliken population analysis indicate that, the bonding of the AlO<sub>2</sub>-Al-OT interface is mainly covalent, and that of the LaO-OT interface is a mixture of covalent bond, ionic bond and metallic bond, while that of the AlO<sub>2</sub>-O-OT interface is covalent and ionic. (3) Interface magnetism analysis indicates that, for the AlO<sub>2</sub>-Al-OT and AlO<sub>2</sub>-O-OT interfaces, the spin magnetic moments of Ni atoms are both larger than that of the bulk Ni. It indicates that the

formation of AlO<sub>2</sub>-terminated interface enhances the polarization of Ni atom. For the LaO-OT interface, the magnetic moment of Ni atom differs slightly from that of the bulk Ni. However, the magnetic moment of Ni atom of the LaO-MT interface is far less than that of the bulk Ni, which indicates that the formation of LaO-MT interface reduces the polarization of Ni atom. (4) When  $\Delta\mu_{Al}$  is low, the LaO-terminated interface is more stable than the AlO<sub>2</sub>-terminated interface. When  $\Delta\mu_{Al}$  is high, the AlO<sub>2</sub>-terminated interface becomes more stable. Besides, for the AlO<sub>2</sub>-terminated interface, the AlO<sub>2</sub>-O-OT interface is more stable than the AlO<sub>2</sub>-Al-OT one. While for the LaO-terminated interface, the LaO-OT interface is more stable. (5) For the four LaAlO<sub>3</sub>/Ni interfaces, when  $\Delta\mu_{Al}$  is less than  $-14.15$  eV and  $-11.74$  eV, the interfacial energy of the LaO-MT interface and LaO-OT interface is smaller than the liquid/solid interfacial energy of Ni ( $\sigma_{Ni(l)/Ni(s)}$ ), respectively. When  $\Delta\mu_{Al}$  is more than  $-9.09$  eV and  $-6.63$  eV, the interfacial energy of the AlO<sub>2</sub>-O-OT and AlO<sub>2</sub>-Al-OT interfaces is smaller than  $\sigma_{Ni(l)/Ni(s)}$ , respectively. Therefore, LaAlO<sub>3</sub> can be the heterogeneous nucleus of Ni and refine Ni grains.

#### Acknowledgments

The authors acknowledge financial support by the National Natural Science Foundation of China under the Contract Nos. 51271163 and 51471148, and the Hebei Province Basic Research Foundation of China under the Contract No. 16961008D.

#### References

- [1] Q.S. Ma, Y.J. Li, J. Wang, K. Liu, Microstructure evolution and growth control of ceramic particles in wide-band laser clad Ni60/WC composite coatings, *Mater. Des.* 92 (2016) 897–905.
- [2] Z.K. Weng, A.H. Wang, X.H. Wu, Y.Y. Wang, Z.X. Yang, Wear resistance of diode laser-clad Ni/WC composite coatings at different temperatures, *Surf. Coat. Technol.* 304 (2016) 283–292.
- [3] K. Liu, Y.J. Li, J. Wang, In-situ reactive fabrication and effect of phosphorus on microstructure evolution of Ni/Ni<sub>3</sub>Al intermetallic composite coating by laser cladding, *Mater. Des.* 105 (2016) 171–178.
- [4] Z. Shafiee, M.E. Bahrololoom, B. Hashemi, Electrodeposition of nanocrystalline Ni/Ni-Al<sub>2</sub>O<sub>3</sub> nanocomposite modulated multilayer coatings, *Mater. Des.* 108 (2016) 19–26.
- [5] T. Liyanage, G. Fisher, A.P. Gerlich, Microstructures and abrasive wear performance of PTAW deposited Ni-WC overlays using different Ni-alloy chemistries, *Wear* 274–275 (2012) 345–354.
- [6] L. Benea, S.B. Basa, E. Danaila, N. Caron, O. Raquet, P. Ponthiaux, J.P. Celis, Fretting and wear behaviors of Ni/nano-WC composite coatings in dry and wet conditions, *Mater. Des.* 65 (2015) 550–558.
- [7] S.P. Sharma, D.K. Dwivedi, P.K. Jain, Effect of La<sub>2</sub>O<sub>3</sub> addition on the microstructure, hardness and abrasive wear behavior of flame sprayed Ni based coatings, *Wear* 267 (2009) 853–859.
- [8] P. Farahmand, R. Kovacevic, Corrosion and wear behavior of laser clad Ni-WC coatings, *Surf. Coat. Technol.* 276 (2015) 121–135.
- [9] K.L. Wang, Q.B. Zhang, M.L. Sun, X.G. Wei, Y.M. Zhu, Rare earth elements modification of laser clad nickel based alloy coatings, *Appl. Surf. Sci.* 174 (2001) 191–200.
- [10] K.L. Wang, Q.B. Zhang, M.L. Sun, X.G. Wei, Y.M. Zhu, Microstructure and corrosion resistance of laser clad coatings with rare earth elements, *Corros. Sci.* 43 (2001) 255–267.
- [11] Z.Y. Zhang, Z.P. Wang, B.N. Liang, H.B. Dong, S.V. Hainsworth, Effect of CeO<sub>2</sub> on the microstructure and wear behavior of thermal spray welded NiCrWRE coatings, *Wear* 262 (2007) 562–567.
- [12] T. Zhao, X. Cai, S.X. Wang, S.A. Zheng, Effect of CeO<sub>2</sub> on microstructure and corrosive



- wear behavior of laser-cladded Ni/WC coating, *Thin Solid Films* 379 (2000) 128–132.
- [13] Z. Zhang, Z. Wang, B. Liang, Tribological properties of flame sprayed Fe-Ni-RE alloy coatings under reciprocating sliding, *Tribol. Int.* 39 (2006) 1462–1468.
- [14] Y.F. Han, Y.B. Dai, D. Shu, J. Wang, B.D. Sun, First-principles calculations on the stability of Al/TiB<sub>2</sub> interface, *Appl. Phys. Lett.* 89 (2006) 144107.
- [15] J. Yang, P.F. Zhang, Y.F. Zhou, X.L. Xing, X.J. Ren, Y.L. Yang, Q.X. Yang, Mechanical properties of the hardfacing alloys with different La<sub>2</sub>O<sub>3</sub> additives and the mechanism analysis by first-principles calculations, *Mater. Sci. Eng. A* 591 (2014) 82–89.
- [16] H.L. Zhang, Y.F. Han, Y.B. Dai, J. Wang, B.D. Sun, An ab initio molecular dynamics study: liquid-Al/solid-TiB<sub>2</sub> interfacial structure during heterogeneous nucleation, *J. Phys. D: Appl. Phys.* 45 (2012) 455307.
- [17] K. Li, Z.G. Sun, F. Wang, N.G. Zhou, X.W. Hu, First-principles calculations on Mg/Al<sub>4</sub>C<sub>3</sub> interfaces, *Appl. Surf. Sci.* 270 (2013) 584–589.
- [18] J. Yang, J.H. Huang, D.Y. Fan, S.H. Chen, X.K. Zhao, LaAlO<sub>3</sub> as the heterogeneous nucleus of ferrite: experimental investigation and theoretical calculation, *J. Alloys Compd.* 683 (2016) 357–369.
- [19] Y.F. Zhou, Y.L. Yang, X.W. Qi, Y.W. Jiang, J. Yang, X.J. Ren, Q.X. Yang, Influence of La<sub>2</sub>O<sub>3</sub> addition on microstructure and wear resistance of Fe/Cr/C cladding formed by arc surface welding, *J. Rare Earths* 30 (2012) 1069–1074.
- [20] J.P. Perdew, K. Burke, M. Ernzerhof, Generalized gradient approximation made simple, *Phys. Rev. Lett.* 77 (1996) 3865–3868.
- [21] N. Troullier, J.L. Martins, Efficient pseudopotentials for plane-wave calculations, *Phys. Rev. B* 43 (1991) 1993–2006.
- [22] H.J. Monkhorst, J.D. Pack, Special points for Brillouin-zone integrations, *Phys. Rev. B* 13 (1976) 5188–5192.
- [23] T.H. Fischer, J. Almlof, General methods for geometry and wave function optimization, *J. Phys. Chem.* 96 (1992) 9768–9774.
- [24] B.G. Pfrommer, M. Côté, S.G. Louie, M.L. Cohen, Relaxation of crystals with the quasi-Newton method, *J. Comput. Phys.* 131 (1997) 133–140.
- [25] B.C. Chakoumakos, D.G. Schlom, M. Urbanik, J. Luine, Thermal expansion of LaAlO<sub>3</sub> and (La,Sr)(Al,Ta)O<sub>3</sub>, substrate materials for superconducting thin-film device applications, *J. Appl. Phys.* 83 (1998) 1979–1982.
- [26] X. Luo, B. Wang, Y. Zheng, First-principles study on energetics of intrinsic point defects in LaAlO<sub>3</sub>, *Phys. Rev. B* 80 (2009) 104115.
- [27] C. Kittel, *Introduction to Solid State Physics*, Wiley Interscience, New York, 1986.
- [28] Y. Wang, Z.K. Liu, L.Q. Chen, Thermodynamic properties of Al, Ni, NiAl, and Ni<sub>3</sub>Al from first-principles calculations, *Acta Mater.* 52 (2004) 2665–2671.
- [29] R.S. Dutta, A. Arya, C. Yusufali, B. Vishwanadh, R. Tewari, G.K. Dey, Formation of aluminides on Ni-based superalloy 690 substrate, their characterization and first-principle Ni(111)/NiAl(110) interface simulations, *Surf. Coat. Technol.* 235 (2013) 741–747.
- [30] A. Ernst, G. van der Laan, W.M. Temmerman, S.S. Dhesi, Z. Szotek, Contesting results for magnetic moments in nickel thin films, *Phys. Rev. B* 62 (2000) 9543.
- [31] J. Boettger, Nonconvergence of surface energies obtained from thin-film calculations, *Phys. Rev. B* 49 (1994) 16798–16800.
- [32] W.R. Tyson, W.A. Miller, Surface free energies of solid metals: estimation from liquid surface tension measurements, *Surf. Sci.* 62 (1977) 267–276.
- [33] X.G. Wang, A. Chaka, M. Scheffler, Effect of the environment on  $\alpha$ -Al<sub>2</sub>O<sub>3</sub> (0001) surface structures, *Phys. Rev. Lett.* 84 (2000) 3650–3653.
- [34] J. Li, M. Zhang, Y. Zhou, G.X. Chen, First-principles study of Al/Al<sub>13</sub>Ti heterogeneous

nucleation interface, *Appl. Surf. Sci.* 307 (2014) 593–600.

[35] B.L. Bramfitt, The effect of carbide and nitride additions on the heterogeneous nucleation behavior of liquid iron, *Metall. Mater. Trans. B Process Metall. Mater. Process. Sci.* 1 (1970) 1987–1995.

[36] J. Guo, L.G. Liu, S. Liu, Y.F. Zhou, X.W. Qi, X.J. Ren, Q.X. Yang, Stability of eutectic carbide in Fe-Cr-Mo-W-V-C alloy by first-principles calculation, *Mater. Des.* 106 (2016) 355–362.

[37] Y.J. Xian, R.Z. Qiu, X. Wang, P.C. Zhang, Interfacial properties and electron structure of Al/B<sub>4</sub>C interface: A first-principles study, *J. Nucl. Mater.* 478 (2016) 227–235.

[38] J.R. Smith, W. Zhang, Stoichiometric interfaces of Al and Ag with Al<sub>2</sub>O<sub>3</sub>, *Acta Mater.* 48 (2000) 4395–4403.

[39] M. Christensen, S. Dudiy, G. Wahnström, First-principles simulations of metal-ceramic interface adhesion: Co/WC versus Co/TiC, *Phys. Rev. B* 65 (2002) 045408.

[40] Y.F. Li, Y.M. Gao, B. Xiao, T. Min, S.Q. Ma, D. Yi, Theoretical calculations on the adhesion, stability, electronic structure, and bonding of Fe/WC interface, *Appl. Surf. Sci.* 257 (2011) 5671–5678.

[41] J.H. van der Merwe, Interfacial energy: bicrystals of semi-infinite crystals, *Surf. Sci.* 67 (2001) 365–381.

[42] V.P. Skripov, in: E. Kaldis, H. Scheel (Eds.), *Crystal Growth and Materials*, 1977 North-Holland, Amsterdam.

[43] W. Zhang, J.R. Smith, A.G. Evans, The connection between ab initio calculations and interface adhesion measurements on metal/oxide systems: Ni/Al<sub>2</sub>O<sub>3</sub> and Cu/Al<sub>2</sub>O<sub>3</sub>, *Acta Mater.* 50 (2002) 3803–3816.

**Table 1**Surface energy of LaAlO<sub>3</sub> (100) and Ni (100) surfaces.

Layers, n	Surface energy (J/m <sup>2</sup> )		
	Ni (100)	LaAlO <sub>3</sub> (100)	
		AlO <sub>2</sub> -termination	LaO-termination
3	2.52	-3.33	7.47
5	2.40	-3.39	7.42
7	2.34	-3.44	7.36
9	2.32	-3.43	7.36
11	2.33	-3.44	7.37

**Table 2**Planar lattice misfit between LaAlO<sub>3</sub> and Ni.

Matching interface	(100) <sub>LaAlO<sub>3</sub></sub> //(100) <sub>Ni</sub>		
[uvw] <sub>LaAlO<sub>3</sub></sub>	[010]	[011]	[001]
[uvw] <sub>Ni</sub>	[010]	[011]	[001]
θ	0	0	0
d <sub>LaAlO<sub>3</sub></sub> (Å)	3.838	5.428	3.838
d <sub>Ni</sub> (Å)	3.536	5.000	3.536
δ (%)	8.5		

**Table 3**Interface ideal adhesion energy W<sub>ad</sub> and interfacial separation d<sub>0</sub> for the four LaAlO<sub>3</sub>/Ni interface systems.

Termination	Stacking	Relaxed	
		d <sub>0</sub> /Å	W <sub>ad</sub> /J m <sup>-2</sup>
AlO <sub>2</sub>	Al-OT	2.192	2.24
	O-OT	2.046	3.58
LaO	OT	2.348	3.07
	MT	2.461	1.76

**Table 4**

Mulliken bond population analysis results between the interfacial atoms for the LaAlO<sub>3</sub>/Ni interfaces. OT is on top of the interfacial atom. MT is on top of the middle of interfacial atoms.

Termination	Stacking	Bond	Length (Å)	Population
AlO <sub>2</sub>	Al-OT	Al—Ni(Al—OT)	2.511	0.29
		O—Ni(Al—OT)	2.893	−0.08
		O—Ni(MT)	2.541	0.15
	O-OT	Al—Ni	2.786	0.18
		O—Ni	1.970	0.46
LaO	OT	La—Ni(La—OT)	2.628	−1.04
		O—Ni(O—OT)	2.098	0.22
	MT	La—Ni <sup>a</sup>	—	—
		O—Ni <sup>a</sup>	—	—

<sup>a</sup> The atomic distance is too long to form a chemical bond.

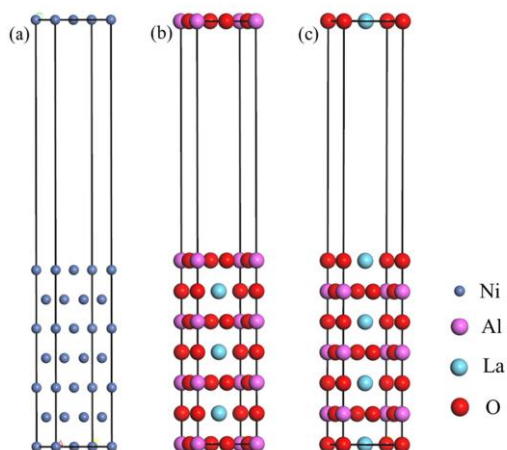


Fig. 1. Crystal Structures of Ni (100) slab and LaAlO<sub>3</sub> (100) slab with 7-layer atoms. (a) Ni, (b) AlO<sub>2</sub>-terminated LaAlO<sub>3</sub>, (c) LaO-terminated LaAlO<sub>3</sub>.

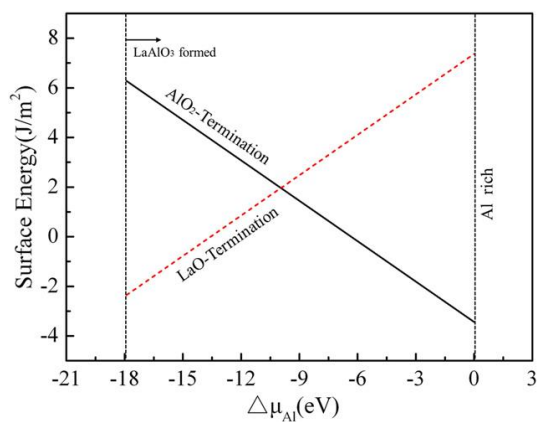


Fig. 2. Surface energy of LaAlO<sub>3</sub> (100) surface as a function of  $\Delta\mu_{\text{Al}}$ .

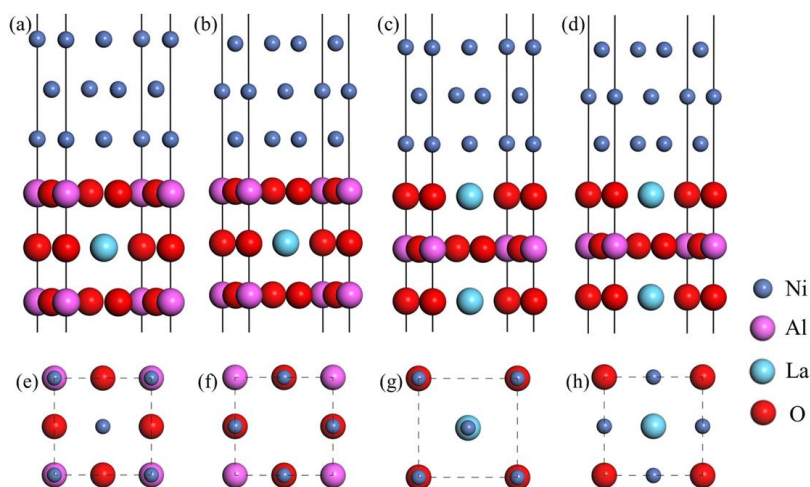


Fig. 3. Crystal Structures of LaAlO<sub>3</sub>(100)/Ni(100) interfaces. (a) AIO<sub>2</sub>-Al-OT interface, (b) AIO<sub>2</sub>-O-OT interface, (c) LaO-OT interface, (d) LaO-MT interface. (e), (f), (g) and (h) are top views of the interfacial atoms corresponding to (a), (b), (c) and (d), respectively.

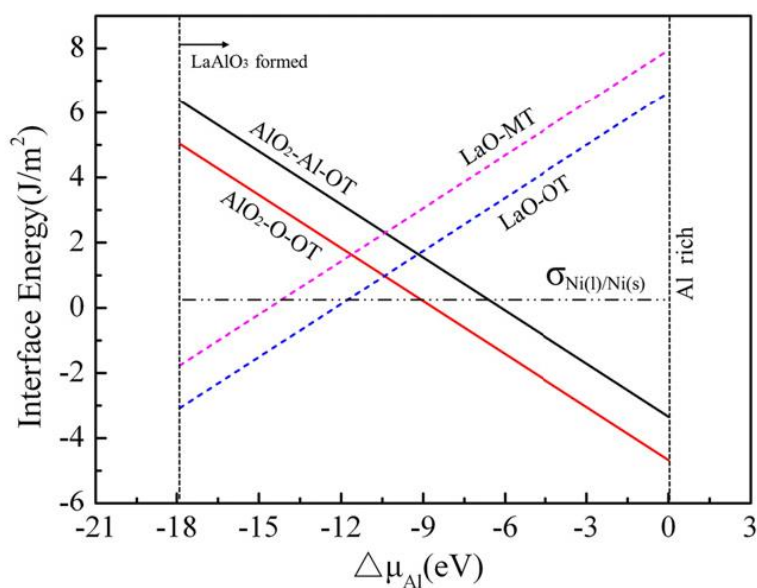


Fig. 4. Interfacial energy for the four LaAlO<sub>3</sub>/Ni interfaces as a function of  $\Delta\mu_{\text{Al}}$ .

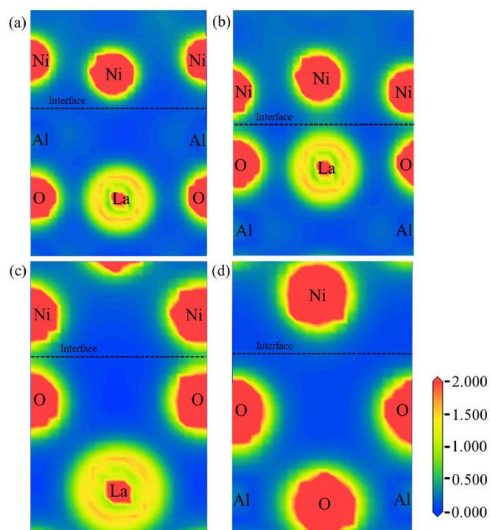


Fig. 5. Charge density for the four LaAlO<sub>3</sub>/Ni interfaces ( $e/\text{\AA}^3$ ). (a) AIO<sub>2</sub>-Al-OT interface along (110) plane, (b) LaO-OT interface along (110) plane, (c) AIO<sub>2</sub>-O-OT interface along (200) plane, (d) LaO-MT interface along (100) plane.

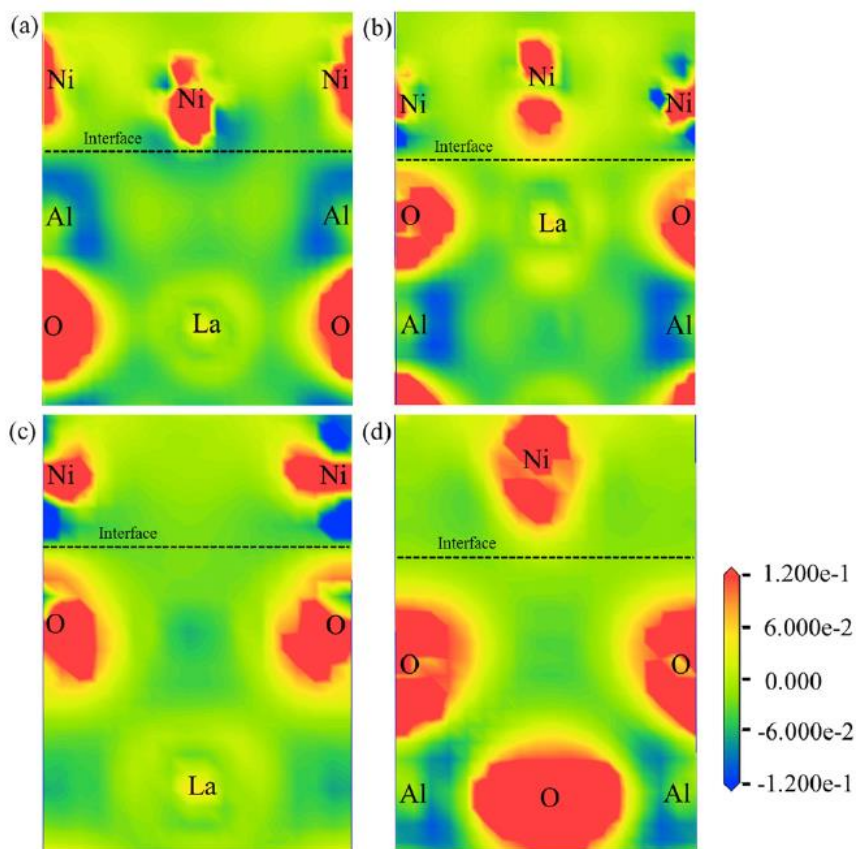


Fig. 6. Charge density difference for the four LaAlO<sub>3</sub>/Ni interfaces ( $e/\text{\AA}^3$ ). (a) AIO<sub>2</sub>-Al-OT interface along (110) plane, (b) LaO-OT interface along (110) plane, (c) AIO<sub>2</sub>-O-OT interface along (200) plane, (d) LaO-MT interface along (100) plane.



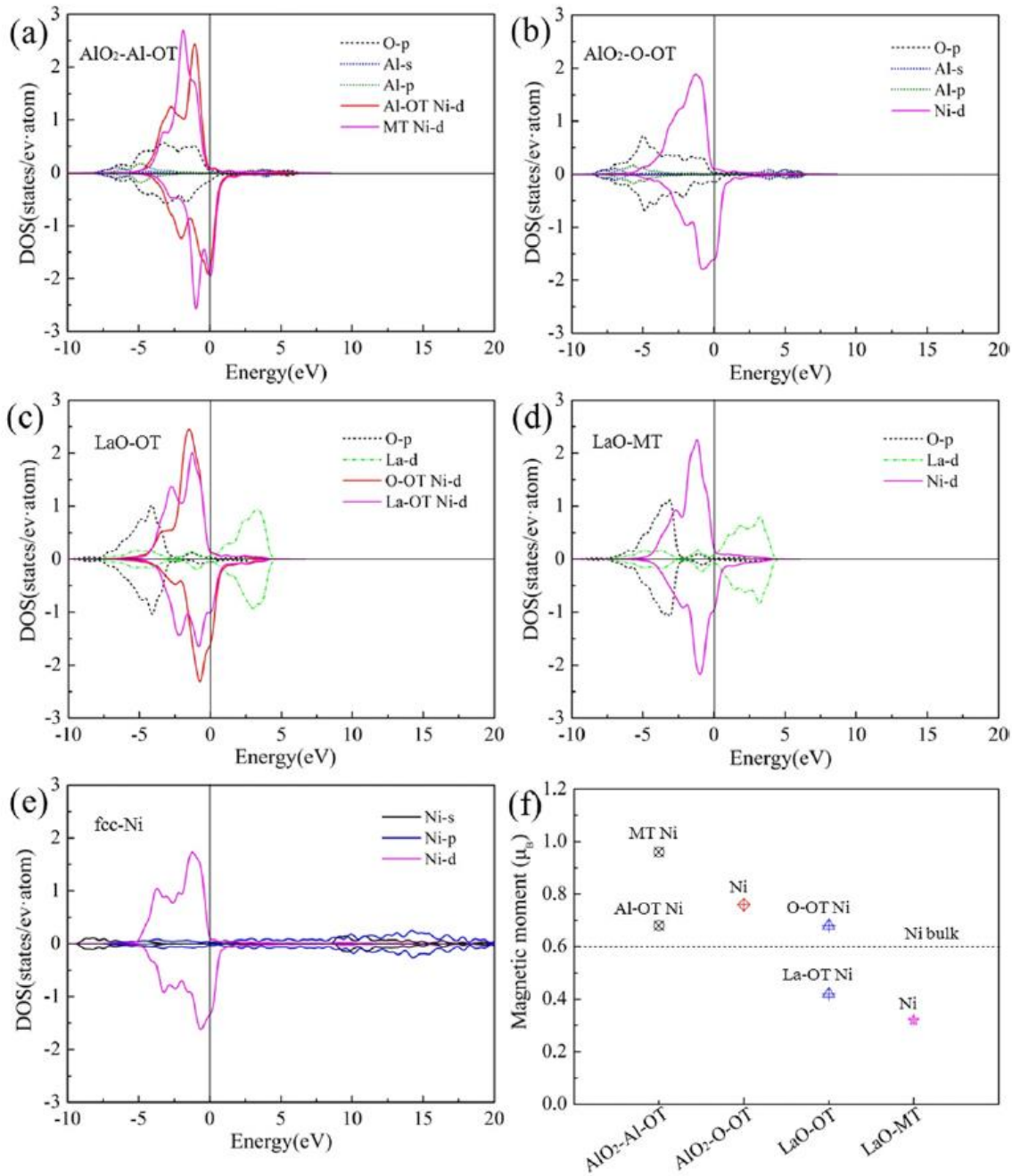


Fig. 7. Spin-polarized layer-projected partial DOS for atoms of (a) AlO<sub>2</sub>-Al-OT interface, (b) AlO<sub>2</sub>-O-OT interface, (c) LaO-OT interface, (d) LaO-MT interface, compared to (e) the bulk Ni partial DOS. (f) Magnetic moments per atom for corresponding Ni atoms of (a), (b), (c), (d) and (e).

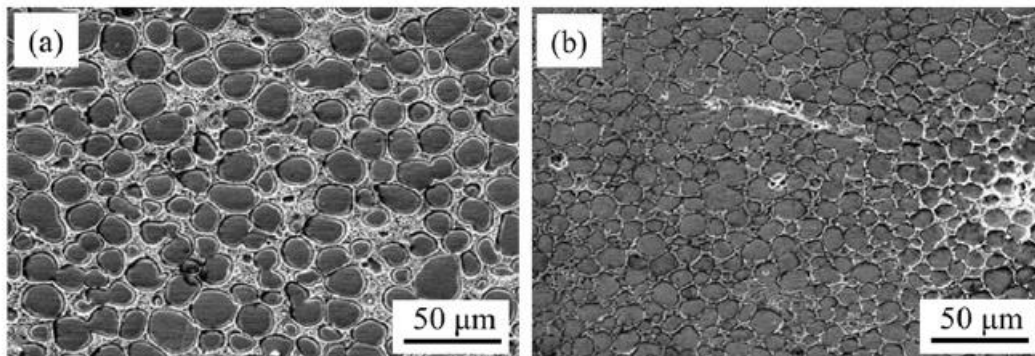


Fig. 8. Microstructure of (a) 0 wt.% La<sub>2</sub>O<sub>3</sub> and (b) 1.2 wt.% La<sub>2</sub>O<sub>3</sub> coatings [7].